Vibrational properties and infrared spectra of $Al_xGa_{1-x}As$ systems. II. Order and disorder features in superlattice configuration

M. Bernasconi and L. Colombo*
Scuola Internazionale Superiore di Studi Avanzati (SISSA), Strada Costiera 11, I-34014 Grignano, Trieste, Italy

L. Miglio
Dipartimento di Fisica dell'Università di Milano, via Celoria 16, I-20133 Milano, Italy
(Received 8 October 1990; revised manuscript received 26 December 1990)

Within the framework developed in the preceding paper (referred to herein as paper I) for the homogeneous alloys, we report our calculation of the dynamical properties for $(Al_xGa_{1-x}As)_p/(Al_yGa_{1-y}As)_p$ superlattices. In particular, $\mathrm{Im}\chi_{xx}$, $-\mathrm{Im}\epsilon_{zz}^{-1}$, and reflectivity spectra are evaluated, within a bond-charge-model, mass-defect scheme, for superlattice periods corresponding to $p=5$ and $p=3$. Compositional disorder has been treated both by an average-t-matrix approximation and a supercell calculation. Features arising from the compositional disorder, structures originating from the superlattice configuration, and their interactions are discussed.

I. INTRODUCTION

Recent investigations on the lattice dynamics of $\langle 001 \rangle$ GaAs/AlAs superlattices[1] provide an exhaustive interpretation of phonon spectra in these systems. By considering the reduction of the original bcc Brillouin zone along the growth direction ($\langle 001 \rangle$), we have a folding of the relative acoustic branches with small gaps opening at the superlattice zone boundary and zone center. At the latter, several acoustic folded vibrations (now true optical modes of the supercell) become Raman or infrared active, depending on their displacement pattern (character). These folded modes propagate all along the growth direction, since both GaAs and AlAs slabs match the frequency and wave-vector conditions (both materials display nearly the same acoustic dispersion relations along $\langle 001 \rangle$).

In the high-frequency side, on the contrary, the optical branches for bulk AlAs and GaAs are well separated in frequency, so that the vibrations taking place in one slab are not allowed to penetrate into the other. This situation gives rise to the confinement of the optical modes in either the GaAs side or the AlAs side. Confined modes are obviously dispersionless along the growth direction and display vanishing amplitude at the interfaces between the two materials: They originate either Raman or infrared activity, according to the usual symmetry condition at the Γ point. As in the case of folded modes, the frequency position of the latter is sensitive to the widths of the layers that compose the superlattice. The frequency of the confined modes is in fact related to the dispersion relations of the corresponding bulk material: A good rule of thumb is that the envelope function of a zone-center confined mode corresponds to a bulk phonon with an integer number of half wavelengths contained in the effective layer [$p+1$ layers in the case of $(GaAs)_p(AlAs)_p$, since interfacial As is in common]. This rule selects a set of quantized wave vectors according to

$$q=\frac{m\pi}{(p+1)a}, \quad m=1,2,3,\ldots, \tag{1}$$

where a is the lattice constant. The frequency of the superlattice confined phonons can be obtained from the dispersion relations of the bulk GaAs (AlAs) at the wave vector given by Eq. (1). Accordingly, the longitudinal and transverse confined optical vibrations are labeled, respectively, by LO_m and TO_m. By increasing the order m of the confined vibrations the intensity of the corresponding Raman and infrared peaks decrease.

Relation (1), however, breaks down for thin layers ($p=1,2$) and the origin of the disagreement with experimental measurements has been recently addressed to be the compositional disorder which takes place at the interfaces, due to cations interdiffusion.[2] For ultra-thin superlattices this process is overwhelming and turns the superperiodic structure into a homogeneous alloy. For thicker layers the effect has a smaller percentile, still qualitatively twofold: (i) the interfacial disorder makes the effective thickness of the pure GaAs (AlAs) layers smaller; (ii) dynamical features from the mixed crystal region should be expected to contribute to the optical spectrum. This is one reason why, in the present paper, we address the problem of calculating the dynamical properties and the infrared spectra for $Al_xGa_{1-x}As/Al_yGa_{1-y}As$ superlattices.

The concept of phonon-dispersion relations is still valid in $Al_xGa_{1-x}As$ alloys, as recently confirmed by a supercell calculation with *ab initio* force constants by Baroni, de Gironcili, and Giannozzi.[3] The dispersion of GaAs-like longitudinal mode in $Al_xGa_{1-x}As$ alloys has been measured by Jusserand, Paquet, and Mollot[4] in the Raman spectrum of the $AlAs/Al_xGa_{1-x}As$ superlattice [making use of Eq. (1) for GaAs-like confined phonons]. Consequently, it is quite interesting to investigate either the validity of relation (1) in $Al_xGa_{1-x}As/Al_yGa_{1-y}As$ systems and the relationship

between superlattice confined modes and the homogeneous alloy dispersion relations. Moreover, as discussed in the preceding paper[5] (hereafter referred to as paper I), the optical modes of homogeneous mixed crystals shift in frequency with Al content, so that the two slabs composing the superlattice cell may display either a separation or a superposition of these branches, depending on $\Delta c = |x - y|$.[6] Confined and extended optical vibrations are thus possible, as in the case of other superlattices, such as InAs/GaSb and Si/Ge,[7] but for the possibility of tuning the Δc parameter. This is one aspect of the general problem that springs out in $Al_xGa_{1-x}As/Al_yGa_{1-y}As$ systems, i.e., to understand which features are amenable to the compositional disorder within each slab, which ones are originating from the superperiodic order, and which effects are produced by the interplay between them.

In order to make a prediction for experimental measurements we have calculated the dielectric function and reflectivity in the spectral region of lattice vibrations. From these response functions we can obtain the excitation spectra for transverse and longitudinal phonons which are detectable by transmission and Raman experiments, respectively (see Sec. VI of paper I). As a by product, we show that a dynamical characterization of a mixed-crystal superlattice is at hand, by considering the qualitative modifications in the optical spectra for these systems when x, y, or the thickness of the slabs are varied.

II. CALCULATION PROCEDURE

The dynamical model here adopted is the bond-charge model (BCM) for GaAs, where the Al impurities are treated in the mass-defect approximation: The reliability of this approach has been extensively discussed in paper I, for the case of homogeneous alloys. Even compositional disorder has been considered in the same framework, i.e., both by an average-t-matrix approximation (ATA) and a supercell calculation (SC). In Secs. IV and V of paper I we have given a detailed description of these methods applied to $Al_xGa_{1-x}As$: Here we just add some remarks concerning the inclusion of the superlattice periodicity. In the ATA approach, the formulas outlined in paper I are still valid but for the index l which is now referred to as the superlattice unit cell and the index κ which is split into $(\bar{\kappa}\bar{l})$, where $\bar{\kappa}$ labels the cation ($\bar{\kappa}=1$) and anion ($\bar{\kappa}=2$) sublattices and $\bar{l}$ labels the bulk unit cells contained in the superlattice one. The averaged Green function and the reference Green function $\vec{G}_0$ display now the $\langle 001 \rangle$ superperiodicity. $\vec{G}_0$ represents a perfect superlattice with cationic masses (depending on $\bar{l}$) in agreement with the virtual crystal approximation. Moreover, it is calculated on the same mesh in the reciprocal space as in paper I, but the Brillouin zone is now the one pertaining to the superlattice. The single-site-scattering procedure is then developed as usual, taking into account the $\bar{l}$ extra index.

An important tool for discriminating either confined or extended modes is the site-projected, weighted phonon density:

$$\rho^i_{Al}(\bar{l},\omega) \sim \omega \frac{\mathrm{Im}\langle G^{ii}_{dd}(1\bar{l},1\bar{l}|q_z \to 0,\omega)\rangle}{c(\bar{l})}, \tag{2a}$$

$$\rho^i_{Ga}(\bar{l},\omega) \sim \omega \frac{\mathrm{Im}\langle G^{ii}_{hh}(1\bar{l},1\bar{l}|q_z \to 0,\omega)\rangle}{[1-c(\bar{l})]} \tag{2b}$$

$$\rho^i_{As}(\bar{l},\omega) \sim \omega\, \mathrm{Im}\langle G^{ii}(2\bar{l},2\bar{l}|q_z \to 0,\omega)\rangle, \tag{2c}$$

where i is the Cartesian index x or z, $c(\bar{l})$ is the Al concentration in the $\bar{l}$ plane, and $\langle \vec{G}_{dd} \rangle$ and $\langle \vec{G}_{hh} \rangle$ are the Fourier transforms of conditional averaged Green functions.[8] These projected densities provide the average mean-square displacements of each atomic species in every plane. With regard to the SC approach the supercell has been taken as long as the superlattice unit cell in the $\langle 001 \rangle$ direction (20 atomic planes for the $p=5$ case) and includes 36 atoms in the plane perpendicular to it (this amounts to 360 small unit cells, i.e., 720 atoms in total for the $p=5$ case). The fact that our supercell encomprises only one superlattice unit cell along the growth direction restricts our analysis just to the $q_z=0$ vibrations: In this case we are actually considering the displacement patterns with a periodicity along $\langle 001 \rangle$ that is just the same as the structural periodicity. This is not a shortcoming, since we are interested in the optical response at the zone center. Configurational average has been performed over a set of six different configurations, where particular attention has been paid to retain the same Al percentage at every plane within each slab.

Some final comment deserves the evaluation of the dielectric functions, already defined in Sec. VI of paper I. In the case of superlattice configuration, the electronic part of the dielectric function is now taken as an average between the two slabs:

$$\epsilon^{\infty}_{xx} = \tfrac{1}{2}(\epsilon^1_{\infty} + \epsilon^2_{\infty}), \tag{3}$$

where 1 and 2 label the two slabs with different Al percentage (each one derived as in the case of homogeneous alloy—see Eq. I-19). In this way the transverse component of the dielectric function is readily evaluated as

$$\epsilon_{xx} = \epsilon^{\infty}_{xx} + 4\pi\chi_{xx}(q_z \to 0)\ . \tag{4}$$

In the case of longitudinal component, we have as well

$$\epsilon_{zz} = \epsilon^{\infty}_{zz} + 4\pi\chi_{zz}(q_z \to 0) \tag{5}$$

with

$$\frac{1}{\epsilon^{\infty}_{zz}} = \frac{1}{2}\left[\frac{1}{\epsilon^1_{\infty}} + \frac{1}{\epsilon^2_{\infty}}\right]. \tag{6}$$

The susceptibility tensor $\vec{\chi}$ has been calculated by means of Eq. (17) in paper I, where the macroscopic electric field has been removed from the Green function [see discussion following Eq. (15) of paper I]. So we actually calculate

$$-\mathrm{Im}\frac{1}{\epsilon_{zz}} = -\mathrm{Im}\frac{1}{\epsilon^{\infty}_{zz} + 4\pi\chi_{zz}(q_z \to 0)} \tag{7}$$

which gives us an optical response that can be helpfully

compared with the Raman $z(xy)\bar{z}$ spectra, but for the relative intensities of the peaks. In the superlattice configuration the disorder in the effective charge Z has been introduced assuming that the cations have the bulk value, as defined in Sec. VI of paper I. On the other hand, the effective charge of As has been calculated in accordance to the virtual-crystal approximation, namely, by averaging the effective charges of neighboring metallic planes. In the SC calculation scheme, we have tested an alternative definition of Z_{As}: We assigned to each As ion the average of the effective charges of its nearest neighbors. It turns out that the two different models produce the same dielectric function, in the optical region. Here we present the results obtained by the former definition for the As effective charge.

III. RESULTS AND DISCUSSION

In the framework of the ATA approach, we have calculated $\mathrm{Im}\chi_{xx}$, $-\mathrm{Im}\epsilon_{zz}^{-1}$ and reflectivity spectra of $(Al_xGa_{1-x}As)_p(Al_yGa_{1-y}As)_p$ superlattices in the following configurations.

For $p=5$

$x=0.2$, $y=0.8$,

$x=0.2$, $y=0.4$,

$x=0.1$, $y=0.4$;

for $p=3$,

$x=0.2$, $y=0.8$.

Here we report only the most interesting spectra, and compare them to the corresponding $(GaAs)_p(AlAs)_p$ ones. Moreover, we display also the normalized superposition of the optical spectra for the corresponding homogeneous alloys $\frac{1}{2}(Ga_xAl_{1-x}As)+\frac{1}{2}(Ga_yAl_{1-y}As)$, which simulates an incoherent mixture of the two materials. In this way, disorder-activated structures can be compared and the effects of superperiodic order are easily pointed out. SC results are reported only for a limited set of spectra, where the ATA calculations indicate that interesting features deserve a check by a nonperturbative treatment of the compositional disorder. Because of the similarities in the effective charges between Ga and Al, disorder-activated and folded transverse acoustic (DATA and FTA, respectively) modes and their longitudinal counterparts (DALA and FLA) are very weak. All figures are enhanced by a factor 100 (20 in some cases) in the acoustic region in order to put them in evidence. These structures are conversely stronger in Raman spectra since the electronic polarizabilities of AlAs and GaAs are sensibly different. Extensive calculations in the framework of ATA-BCM (and SC-BCM as well) and the bond polarizability model for the Raman $z(xy)-z$ intensity of Al-Ga-As superlattices and modulated alloys will be reported in a forthcoming publication of ours.[9]

How do we expect the $\mathrm{Im}\chi_{xx}$ and $-\mathrm{Im}\epsilon_{zz}^{-1}$ spectra for $(Al_xGa_{1-x}As_p(Al_yGa_{1-y}As)_p$ to come out? In the acoustic region (up to 6 THz) either FTA or FLA modes should be superimposed to the DATA and DALA broad bands, as long as the difference in Al percentage between the two slabs makes the superlattice order effective. In the optical side, the $(Al_xGa_{1-x}As)_p$ slab should contribute with both GaAs-like and AlAs-like modes, and the $(Al_yGa_{1-y}As)_p$ slab as well. Both in $\mathrm{Im}\chi_{xx}$ and $-\mathrm{Im}\epsilon_{zz}^{-1}$ spectra, $p+1(p=\text{odd})$ AlAs-like and GaAs-like peaks should appear since only the vibrations with displacement patterns displaying an odd number of half-wavelengths in the slab are active (that is, confined modes of order 1 and 3 are allowed for $p=3$ and that of order 5 is added in case of $p=5$). However, this would happen just in case that all the optical modes turn out to be confined. Due to the partial frequency superposition between the two slabs, some vibrations may come out propagative and the final number of resolved peaks is drastically reduced.

In Fig. 1(a) we compare $\mathrm{Im}\chi_{xx}$ for the normalized superposition of two homogeneous alloys, corresponding to $x=0.2$ and $x=0.8$ (top panel: 20+80), with the corresponding superlattice configuration, $p=5$, $x=0.2$, $y=0.8$ (central panel: 20/80), and with the $(GaAs)_5(AlAs)_5$ superlattice (bottom panel: 0/100). In the acoustic region we note that the 20/80 configuration displays a superposition of DALA and DATA modes with some FTA (label *F*), coming from the $p=5$ superperiodicity. Modifications of the phonon spectrum in the coustic region, due to the superperiodicity, originate a slight modification of DATA structure beyond 3 THz. In the optical part of the 0/100 panel we note TO_1, TO_3, and TO_5 AlAs- and GaAs-confined modes. Al-rich , Al-poor (between 10 and 11 THz), and Ga-rich, Ga-poor (below 8 THz) peaks are characteristic of the incoherent superposition of the panel 20+80. The mixed crystal superlattices 20/80 display two confined modes (TO_1-like) for Ga-rich and Al-rich sides (label *C*): Confined modes are found to follow Eq. (1) for the dispersion relations of the corresponding alloy only if the ratio between the mean-square displacement of atoms in the two slabs is approximately larger than 20 (true confined modes, labeled *C* in all the figures). The difference in frequency between the TO_1 mode in 0/100 and the TO_1-like (*C*) mode in the 20/80 spectra is thus attributed to the shift of the optical branch with the Al percentage, as discussed in paper I. For $p=5$ in the 20/80 configuration, the TO_1Ga-poor and TO_3 Ga-rich confined peaks, obtained from Eq. (1), are nearly superimposed; the same is true for TO_1 Al-poor and TO_3 Al-rich peaks, so that modes traveling through the whole superlattice appear in the 20/80 configuration. Their displacement patterns show a superposition of confined modes (vanishing at the interface) TO_1-like and TO_3-like in the poor and rich side, respectively. Since the dipolar activity in the two slabs is opposite, the overall result for the entire superlattice is a quenching of the infrared response at these frequencies (label *Q*) with respect to the 20+80 configuration. The latter effect is not peculiar to mixed crystal superlattices, since, in principle, other superlattices made out of different materials with partially overlapping optical bands may display the same situation.[7] However, the tunability of the frequency positions with Al percentage makes Al-Ga-As superlattices very suitable systems for tailoring this effect.

Figure 1(b) displays the SC result for the 20/80 system: We see that the overall agreement is very satisfactory.

The acoustic part of the spectra is quite similar and the optical peaks are well reproduced considering their intensity. We remark that it is hard to identify the folded acoustic modes in the SC calculations. As a matter of fact, the DALA and DATA modes reproduce the DOS which, in the SC calculations, turns out to be computed with a relatively coarse mesh of the Brillouin zone (the coarseness depends on the size of the SC). On the other hand, the weaker structures in the optical region [which broaden the AlAs-like quenced structure (Q), clearly visible in the ATA spectrum] are due to the presence of clusters in the SC, as already commented in the case of a homogeneous alloy.[5] We are confident that one could reduce these weaker structures by increasing the number of configuration used for the average (six in the present work). The ATA optical peaks are slightly shifted in frequency with respect to the SC ones: This result is simply due to a lower numerical accuracy of the smaller computer on which the ATA calculations have been performed and has no physical origin.[10]

In order to study effect of changing the superperiodic length, we report in Figs. 2(a) and 2(b) an ATA and SC calculation, respectively, of 20/80 systems for $p=3$. Here we note a major separation of the two AlAs-like structures and a shift to lower frequency of the entire op-

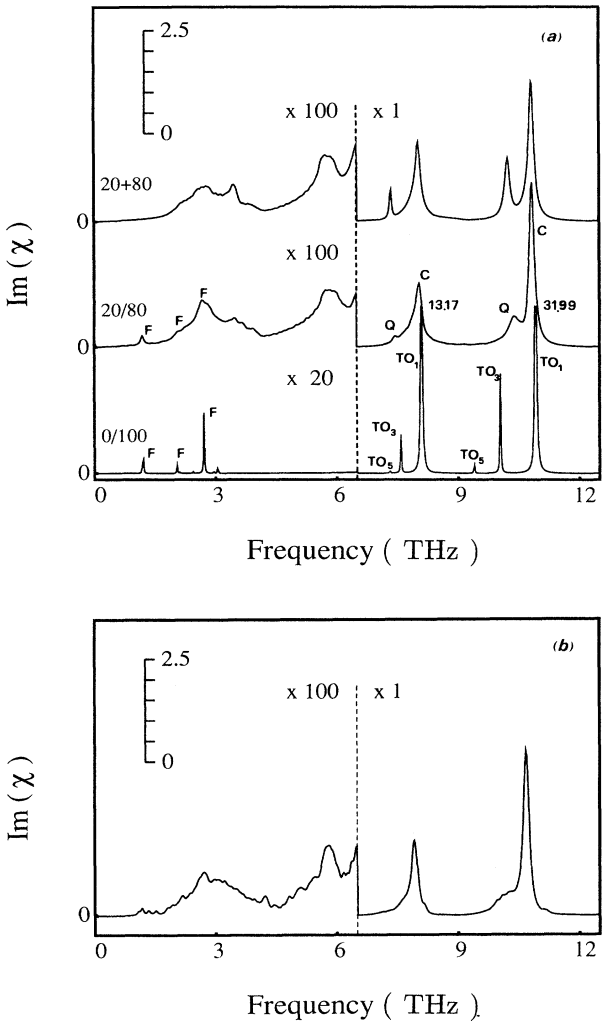

FIG. 1. (a) ATA $\mathrm{Im}\chi_{xx}$ spectra for GaAs/AlAs superlattice (0/100 bottom panel), $(Al_xGa_{1-x}As)_p/(Al_yGa_{1-y}As)_p$ superlattices with $p=5$, $x=0.2$, and $y=0.8$ (20/80 central panel), and normalized sum of the homogeneous alloy (20+80 top panel). Folded (label F), true confined (label C), and quenched (label Q) modes are indicated in the 20/80 spectrum. TO_m GaAs and AlAs peaks are marked in the 0/100 panel. The absolute intensity of the truncated optical peaks has been explicitly indicated. The spectra have been magnified by a factor 100 (central and top panel) or 20 (bottom panel) for frequencies below 6.5 THz. The scale for the vertical axis is reported in the top left corner of the figure. (b) SC $\mathrm{Im}\chi_{xx}$ spectrum for $(Al_xGa_{1-x}As)_p/(Al_yGa_{1-y}As)_p$ superlattices with $p=5$, $x=0.2$, and $y=0.8$. The supercell contains one period in the $\langle 001 \rangle$ direction and 720 atoms in total [36 on each (001) plane].

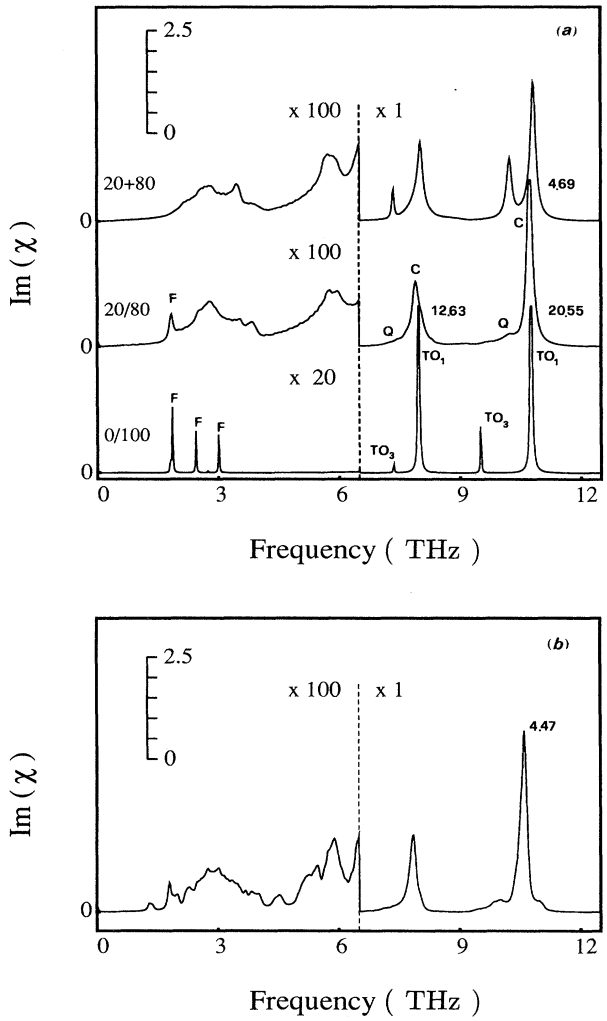

FIG. 2. (a) The same as Fig. 1(a) for a superlattice period corresponding to $p=3$. (b) The same as Fig. 1(b) for a superlattice period corresponding to $p=3$. The supercell contains 432 atoms in total [36 on each (001) plane].

tical spectrum [according to Eq. (1)]. In the acoustic region the FTA peaks change position and intensity [label F in Fig. 2(a)], in agreement with the fact that the folding of the original Brillouin zone is now changed.

In Fig. 3 we report the same configuration of Fig. 1(a) but for a different Al percentage in the two slabs ($x=0.2, y=0.4$) and a smaller $\Delta c=|x-y|$. We note a sizable similarity between the 20/40 panel and the 20+40 one: As a matter of fact, as Δc decreases the superlattice features [folded and strongly confined modes following Eq. (1)] vanish and the two-material system loses memory of the superlattice ordering. Further decreasing of Δc destroys any localization in the system and the spectral line shape approaches the one of a homogeneous alloy with an average Al percentage. Panel 20/40 of Fig. 3 seems to display the latter situation since only one *reststrahlen* peak for AlAs and one for GaAs are visible.

The same physical picture is confirmed by the analysis of longitudinal-mode response. In fact, we display in Figs. 4(a), 4(b), 5, and 6 the $-\mathrm{Im}\epsilon_{zz}^{-1}$ spectra: They are the longitudinal counterparts of Figs. 1(a), 1(b), 2(a), and 3, respectively. Relation to the Raman backscattering spectra can be done, but for the relative intensities of the peaks which deserve a suitable treatment of the polarizability tensor.[9] Figure 4(a) shows sharp FLA peaks in the 20/80 panel, at the same positions of the ones for the 0/100 panel (label F). At variance with respect to the FTA case, they do not superimpose to the DATA band, so that a slight reduction of these disorder-activated structures (as an "ordering" effect) is visible by compar-

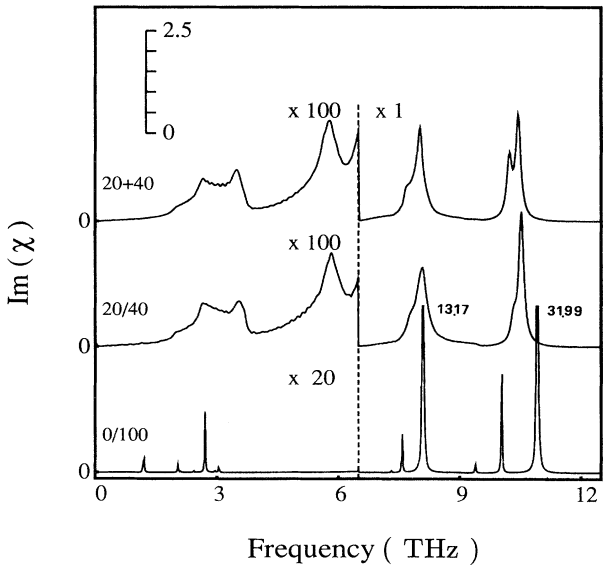

FIG. 3. ATA $\mathrm{Im}\chi_{xx}$ spectra for GaAs/AlAs superlattices (0/100 bottom panel), $(\mathrm{Al}_x\mathrm{Ga}_{1-x}\mathrm{As})_p/(\mathrm{Al}_y\mathrm{Ga}_{1-y}\mathrm{As})_p$ superlattices with $p=5$, $x=0.2$, and $y=0.4$ (20/40 central panel), and normalized sum of the homogeneous alloy (20+40 top panel). The absolute intensity of the truncated optical peaks has been explicitly indicated. the spectra have been magnified by a factor 100 (central and top panel) or 20 (bottom panel) for frequencies below 6.5 THz.

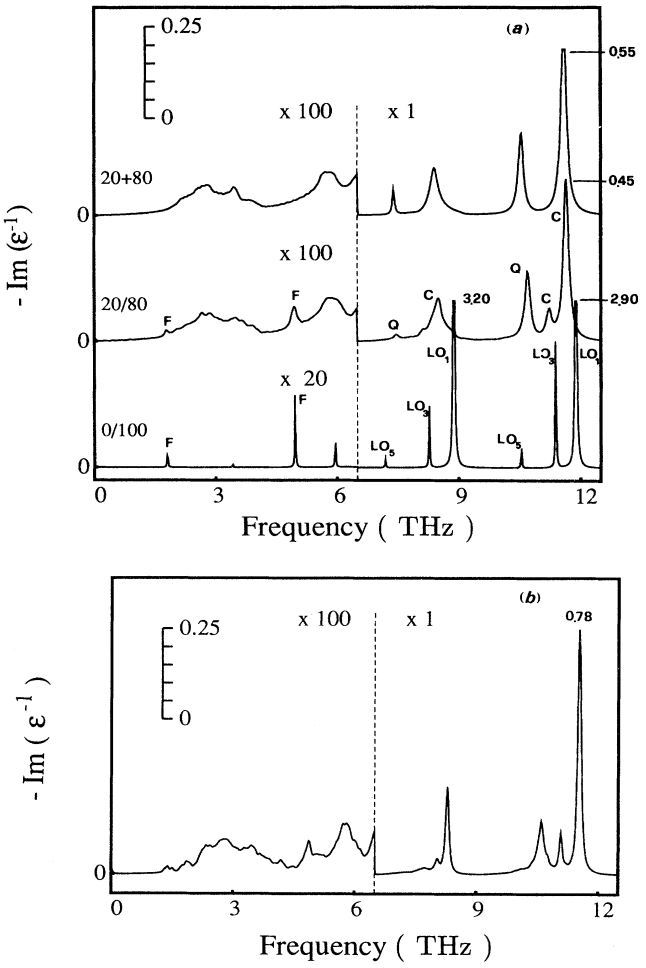

FIG. 4. (a) The same as Fig. 1(a) for the $-\mathrm{Im}\epsilon_{zz}^{-1}$ function. (b) The same as Fig. 1(b) for the $-\mathrm{Im}\epsilon_{zz}^{-1}$ function.

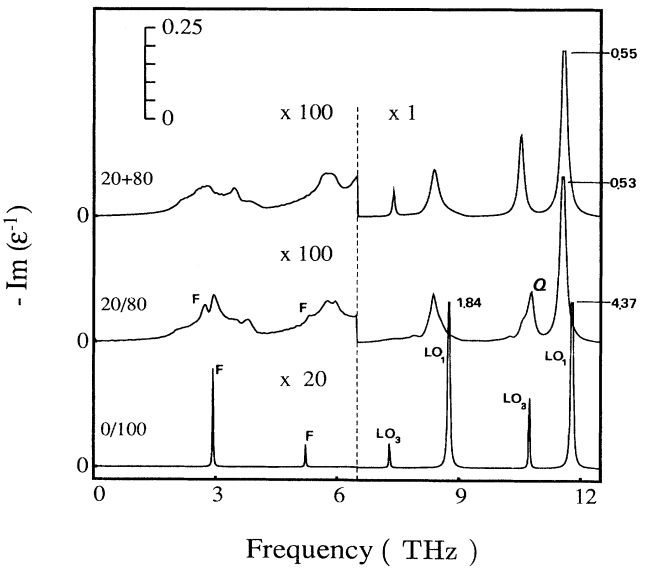

FIG. 5. The same as Fig. 2(a) for the $-\mathrm{Im}\epsilon_{zz}^{-1}$ function.

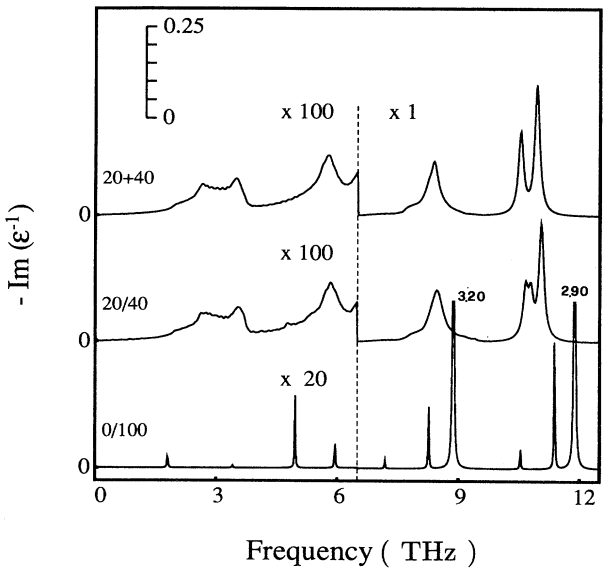

FIG. 6. The same as Fig. 3 for the $-\mathrm{Im}\epsilon_{zz}^{-1}$ function.

ison to the 20+80 panel. In the optical region of 20/80, the AlAs-like peaks of the Al-poor and Al-rich regions are more separated in frequency than the corresponding transverse modes (see Fig. 1). This is a consequence of the dependence on the defect concentration of the macroscopic electric field which affects only the longitudinal vibrations (note also the shift with respect to the pure AlAs LO_1 peak of panel 0/100). This feature makes clearly visible the AlAs-like second quantized LO_3 mode of the Al-rich slab in the spectrum of the alloy superlattice. Moreover, by studying other different superlattice configurations (3/3, 6/4, and 4/6) we found that the LO_3 mode obeys the quantization rule (1) in a very strict way and, consequently, can be use to derive from the experimental Raman spectrum of a $GaAs/Al_xGa_{1-x}As$ superlattice the phonon-dispersion relations of the $Al_xGa_{1-x}As$ homogeneous alloy.[4] Conversely, starting from the dispersion relations, the width of the $Al_xGa_{1-x}As$ slab in a superlattice can be deduced from the frequency position of the LO_3 peak. Finally, we observe the quenching of the low-frequency mode in the GaAs-like region, similar to the case previously discussed for the transverse vibrations (label Q). In this case, the quenching is caused by the matching between LO_1 and LO_5 modes in the two different slabs. Comparison to the 20/80 SC result, Fig. 4(b), is fairly satisfactory and points out the fictitious broadening of GaAs-like structures, induced by the ATA approximation (see paper 1).

In Fig. 5 the ATA calculation is reported for $-\mathrm{Im}\epsilon_{zz}^{-1}$ of the 20/80 system with $p=3$. The LO_3-like mode of the Al-rich slab now falls slightly below the structure originating from the Al-poor region, according to Eq. (1): The superposition of these LO_3-rich and LO_1-poor modes originates a drastic quenching of the LO_1 structure (Q), due to the larger cancellation of dipolar activity with respect to the LO_1-LO_5 superposition of Fig. 4(a). The SC calculation, not reported here, confirms the present analysis. In the acoustic region, the FLA peaks change position and intensity (label F) in agreement with the different dimensions of the Brillouin zone.

In Fig. 6, for the $x=0.2$, $y=0.4$ case, we find that the small Δc strongly reduces the superperiodic effects, as in the case of $\mathrm{Im}\chi_{xx}$ in Fig. 3. At variance with the latter, however, we see that the two peaks corresponding to the Al-rich and Al-poor regions are present and well separated. Moreover, a small splitting places in evidence the presence of the LO_3 Al-rich confined peak, with respect to the LO_1 Al-poor one. Therefore, in the present situation (the 20/40 panel) some degree of confinement is still present in the optical side, even if the acoustic part is nearly equal to the 20+40 incoherent superposition.

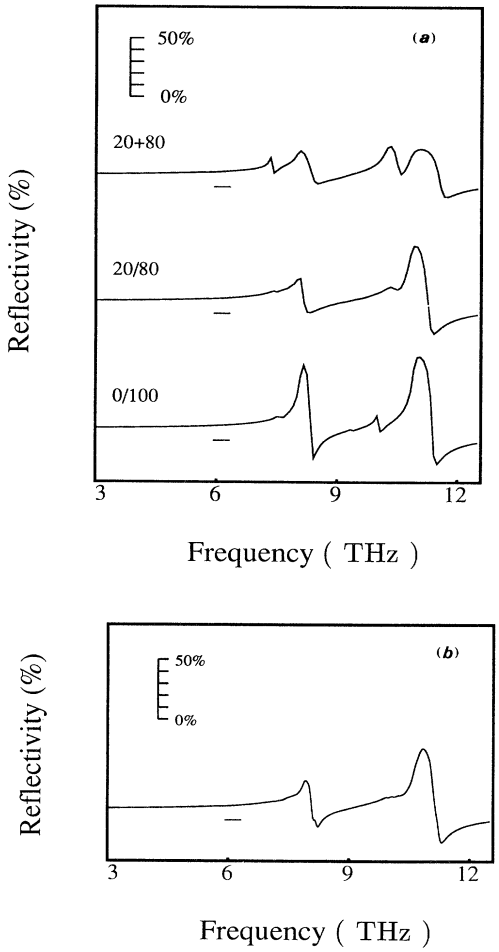

FIG. 7. (a) ATA reflectivity spectra for the GaAs/AlAs superlattice (0/100 bottom panel), $(Al_xGa_{1-x}As)_p/(Al_yGa_{1-y}As)_p$ superlattices with $p=5$, $x=0.2$, and $y=0.8$ (20/80 central panel), and normalized sum of the homogeneous alloy (20+80 top panel). The horizontal bar indicates the 20% reflectivity level. (b) SC reflectivity spectrum for $(Al_xGa_{1-x}As)_p/(Al_yGa_{1-y}As)_p$ superlattices with $p=5$, $x=0.2$, and $y=0.8$. The supercell contains 720 atoms in total [36 on each (001) plane]. The horizontal bar indicates the 20% reflectivity level.

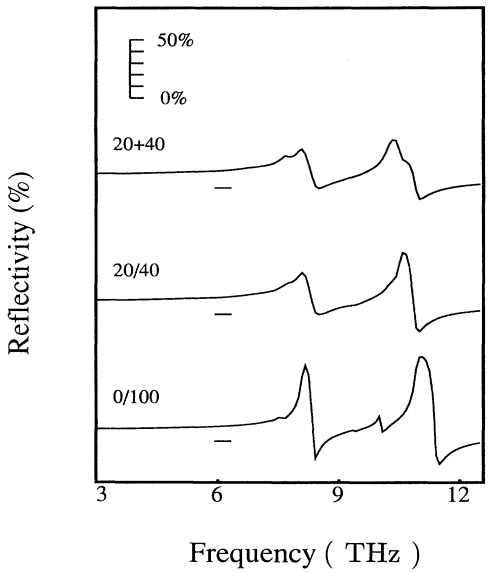

FIG. 8. ATA reflectivity spectra for GaAs/AlAs superlattices (0/100 bottom panel), $(Al_xGa_{1-x}As)_p/(Al_yGa_{1-y}As)_p$ superlattices with $p=5$, $x=0.2$, and $y=0.4$ (20/40 central panel), and normalized sum of the homogeneous alloy (20+40 top panel). The horizontal bar indicates the 20% reflectivity level. The scale for the vertical axis is reported in the top left corner of the figure.

Raman measurements in GaAs/AlAs superlattices with interface disorder[1] have pointed out the presence of structures one order-of-magnitude smaller than DALA and DATA bands, well below the lowest expected FLA and FTA peaks. These structures have been attributed to disorder-activated folded transverse and longitudinal-acoustic modes (DAFTA and DAFLA) originating from the superlattice periodicity (high density of states at zone boundary) and by the compositional disorder at interfaces (zone-center activation of the whole Brillouin zone): a real order-disorder interplay. The similarity in the effective charges between Al and Ga prevents us to resolve DAFTA and DAFLA peaks in Figs. 1–6.[12]

Finally, we present our results for the reflectivity spectra contained in Figs. 7(a) and 7(b) [same configurations of Figs. 1(a) and 1(b) respectively], and Fig. 8 (corresponding to the 20/40 case of Fig. 3). As a matter of fact, it is now hard to extract the same amount of information as in the case of $\mathrm{Im}\chi_{xx}$ and $-\mathrm{Im}\epsilon_{zz}^{-1}$: The reflectivity includes both longitudinal and transverse vibrations and the resulting spectrum is too much integrated to allow for a detailed analysis of the different configurations. Nevertheless, we can see how the reflectivity calculated by ATA and by SC for the 20/80 superlattice [Figs. 7(a) and 7(b), respectively] do agree in intensity but for small kinks aside the main GaAs-like and AlAs-like peaks. The spectra of 20/80 and 20+80 systems [Fig. 7(a)] are much different than in the 20/40 and 20+40 case, according to the general trend given by $\mathrm{Im}\chi_{xx}$ and $-\mathrm{Im}\epsilon_{zz}^{-1}$ in Figs. 1(a), 3, 4(a), and 6. Thus, it turns out that, among the usual experimental techniques, the reflectivity measurements are not suitable for a fruitful investigation of vibrational properties of $(Al_xGa_{1-x}As)_p(Al_yGa_{1-y}As)_p$ superlattices. On the other hand, transmission data and Raman measurements should provide a deeper insight on the general trends occurring in these systems. For what concerns the latter, further calculations in the framework of the bond polarizability model will be published elsewhere.[9]

In conclusion, the major trends occurring in $Al_xGa_{1-x}As/Al_yGa_{1-y}As$ can be outlined as follows: By increasing Δc the dynamical effects of the superperiodicity are enhanced, whereas by decreasing it the system first gives up the superperiodic features (incoherent superposition) and finally drops any information on the two-material structure (averaged homogeneous alloy). In particular, the intensity of FTA and FLA modes increases with Δc, whereas the ones of DATA and DALA decrease with it.

ACKNOWLEDGMENTS

Professor Giorgio Benedek (University of Milano) is gratefully acknowledged for several helpful discussions. Work was partially supported by Consiglio Nazionale delle Ricerche, in the framework of Progetto Finalizzato Materiali Speciali per Tecnologie Avanzate and Comitato Scienze Fisiche for Cray Y-MP calculations.

*Present address: Dipartimento di Fisica, via Celoria 16, I-20133 Milano, Italy.

[1]B. Jusserand and M. Cardona, in *Light Scattering in Solids V*, edited by M. Cardona and G. Güntherodt (Springer, Berlin, 1989), and references cited therein.

[2]E. Molinari, S. Baroni, P. Giannozzi, and S. de Gironcoli, in *Proceedings of the 20th International Conference on the Physics of Semiconductors*, edited by E. M Anastassakis and J. D. Joannopoulos (World Scientific, Singapore, 1990), p. 1429.

[3]S. Baroni, S. de Gironcoli, and P. Giannozzi, Phys. Rev. Lett. **65**, 84 (1990).

[4]B. Jusserand, D. Paquet, and F. Mollot, Phys. Rev. Lett. **63**, 2397 (1989).

[5]M. Bernasconi, L. Colombo, L. Miglio, and G. Benedek, preceding paper, Phys. Rev. B **43**, 14 447 (1991).

[6]B. Jusserand, D. Paquet, and A. Regreny, Phys. Rev. B **30**, 6245 (1984).

[7]A. Fasolino, E. Molinari, and J. C. Maan, Phys. Rev. B **39**, 3923 (1989).

[8]R. J. Elliott, J. A. Krumhansl, and P. L. Leath, Rev. Mod. Phys. **46**, 465 (1974).

[9]C. Molteni, L. Colombo, L. Miglio, G. Benedek, and M. Bernasconi, Philos. Mag. B (to be published); L. Miglio, C. Molteni, and M. Bernasconi (unpublished).

[10]Comparison between the $(GaAs)_5$ $(AlAs)_5$ calculation by Cray Y-MP (used for the SC approach) and the Digital 3100

Workstation (used for the ATA approach) does display the same numerical shift.

[11]J. Sapriel, J. Chavignon, F. Alexandre, and R. Aroulay, Phys. Rev. B **34**, 7118 (1986).

[12]Actually, our very recent calculations of Raman backscattering spectra have pointed out the optical counterparts of DAFTA (i.e., the DAFTO AlAs-like disorder-activated folded transverse-optical structures). In regard to the very low-frequency DAFTA and DAFLA, they fall in a region where numerical fluctuations are large so that Raman peaks from such structures are not resolved.